ChemPubSoc Europe

DOI: 10.1002/cptc.201800031

CHEMPHOTOCHEM Articles

Influence of the Medium on the Photochemical and Photophysical Properties of $[Ru(phen)_2(pPDIp)]^{2+}$**

Isabele Ap. S. de Campos,[a] Edjane R. dos Santos,[a] Tarciso Almeida Sellani,[b] Carolina C. A. Herbozo,[b] Elaine G. Rodrigues,[b] Antonio C. Roveda, Jr.,[c] Wallance M. Pazin,[d] Amando S. Ito,[e] Vinicius T. Santana,[f] Otaciro R. Nascimento,[f] and Rose M. Carlos*[a]

This study reports the influence of the medium on the aggregation processes of the complex $[Ru(phen)_2(pPDIp)]^{2+}$ (phen = 1,10-phenanthroline; pPDIp = a bis-phenanthroline-substituted perylene diimide)and its consequences for the photochemical and photophysical properties of the system. Photolysis leads, initially, to emission of both chromophores: Triplet metal-to-ligand charge transfer (^{3*}MLCT; Ru, dπ→phen, π*) and singlet intraligand charge transfer (^{1*}ILCT; pPDIp, π→ π*). However, the medium induces increased π–π intermolecular interactions that lead to the generation of a $pPDIp^{\bullet-}$moietyin DMSO, $pPDIp^{\bullet-}$ (518 nm) and $pPDIp^{2-}$(420 nm) in the cell culture medium RPMI, and ^{3*}pPDIp in buffer (pH 7.4) and starch films. The complex activates singlet oxygen in buffer solution without oxygen bubbling and under green light irradiation (dose = 0.41J/cm^2; $[^1O_2] = 0.03–0.47$ μmol L^{-1} for $[Ru(phen)_2(pPDIp)]^{2+}$ = 10–150 μmol L^{-1}). No cytotoxic effects on B16F10-Nex2 murine melanoma cell viability were observed up to a concentration of 10 μmol L^{-1} of complex. However, under green LED illumination (dose = 0.41 J/cm^2) the complex exhibits a strong photocytotoxic effect, displaying $IC_{50} = 1.2$ μmol L^{-1}.

1. Introduction

Development of photochemical strategies to generate and detect singlet oxygen ($^1\Delta gO_2$) has attracted much attention because of the potential application of $^1O_2$ in diverse areas of science, particularly in cancer treatment.[1–4] Photodynamic therapy (PDT) is highly recommended in the treatment of superficial and nodular basal cell carcinoma, avoiding surgical excision and skin grafts in the cases where lesions are large.[5–8] For this reason, many photosensitizers based on porphyrins for both systemic administration and topical use have been investigated, and many of them have been approved and are currently available for clinical use in cancer treatments.[9,10]

Metal complexes containing functionalized porphyrazins and phthalocyanines such as those of Pt(II), Pd(II), Cu(II), Mg(II), and Zn(II) have also been investigated, and some have shown encouraging anti-tumor and anti-metastatic properties and are being evaluated in clinical trials.[11–14] Recently, attention has been focused on Ru(II) complexes mostly because some of them have shown favorable pharmacological profiles in vitro and in vivo in different models, including platinum-resistant cell lines.[15–19]

For example, the meso-4-tetrapyridylporphyrin containing four pendant Ru(II)-arene moieties have produced interesting results. Upon light irradiation at 650 nm with a dose of 5 J/cm^2 the complex induced 60–80% mortality in human Me300 melanoma cell cancer at 10 μmol L^{-1} concentration.[18] The polypyridine complexes of Ru(II)-porphyrin containing different bridging linkers have also proved to be effective against cancer activity in HeLa cells, with IC_{50} values between 118 to 175 μmol L^{-1} in the dark and photocytotoxicity at the concentration of 1 μmol L^{-1} upon yellow light irradiation with doses of 6.5 J/cm^2.[19]

The Ru(II)-polypyridine complexes themselves are particularly interesting photosensitizers for PDT because of their unique spectroscopic properties and antitumor activity. They give rise to 100% population of the emissive, long-lived, redox-active triplet state, ^{3*}MLCT, Ru, dπ→π*. They also form adducts with DNA and there are reports of DNA photocleavers with red light illumination.[20]

[a] I. A. S. de Campos, Dr. E. R. dos Santos, Prof. Dr. R. M. Carlos
Departamento de Química
Universidade Federal de São Carlos (UFSCar)
Rodovia Washington Luís, s/n, São Carlos– SP (Brazil)
E-mail: rosem@ufscar.br
[b] T. A. Sellani, C. C. A. Herbozo, Prof. Dr. E. G. Rodrigues
Departamento de Microbiologia, Immunologia e Parasitologia
Escola Paulista de Medicina
Universidade Federal de São Paulo (EPM-UNIFESP)
R. Botucatu 862, 8° andarVila Clementino, São Paulo – SP (Brazil)
[c] Dr. A. C. Roveda, Jr.
Instituto de Química de São Carlos
Universidade de São Paulo (USP)
Av. Trab. São-Carlense, 400Parque Arnold Schimidt, São Carlos – SP (Brazil)
[d] Dr. W. M. Pazin
Departamento de Física
Universidade Estadual Paulista Julio de Mesquita Filho (UNESP)
Rua Roberto Simonsen, 305
Presidente Prudente – SP (Brazil)
[e] Prof. Dr. A. S. Ito
Departamento de Física – FFLRP/USP
Universidade de São Paulo (USP)
Av. Bandeirantes, 3900, Ribeirão Preto – SP (Brazil)
[f] Dr. V. T. Santana, Prof. Dr. O. R. Nascimento
Instituto de Física de São Carlos
Universidade de São Paulo (USP)
Av. Trab. São-Carlense, 400 – Parque Arnold Schimidt
São Carlos– SP (Brazil)

[**] phen = 1,10-phenanthroline; pPDIp = a bis-phenanthroline-substituted perylenediimide derivative.

Supporting information for this article is available on the WWW under https://doi.org/10.1002/cptc.201800031

In this context, we have recently prepared a dyad composed of two chromophores: $\{Ru(phen)_3\}^{2+}$ and perylenediimide (PDI). The $[Ru(phen)_2(pPDIp)]^{2+}$ complex, where phen = 1,10-phenanthroline and pPDIp is a perylene pendant group functionalized with one of the coordinated phenanthroline ligands, shows interesting properties for PDT applications (Figure 1).[21] The key features are intense absorption and

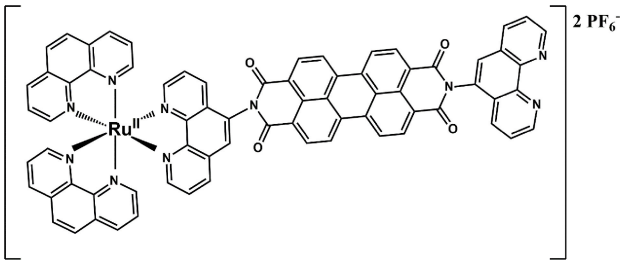

Figure 1. Structure of $[Ru(phen)_2(pPDIp)]^{2+}$ complex.

emission in the visible and near-IR region and long emission lifetime (1.8 μs) originated from the ^{3*}pPDIp component through excitation of the $\{Ru(phen)_3\}^{2+}$ and/or the perylenediimine chromophore in the visible region. The ^{3*}pPDIp sensitizes the formation of singlet molecular oxygen with quantum yield $\phi_\Delta = 0.57$.[21]

This finding motivated us to investigate the dark- and light-cytotoxicity of the $[Ru(phen)_2(pPDIp)]^{2+}$ complex against the B16F10 murine melanoma cells. We choose this cells line, in particular, because of their resistance to many cancer therapies.[22]

A potential phototherapeutic candidate should present biologic and spectroscopic properties compatible with physiologic medium. In general, perylenediimide derivatives present low solubility and a tendency to aggregate in aqueous buffer (pH 7.4) solution, resulting in decreased or total loss of their photochemical activity. This behavior can be minimized with bulk substituents at the bay and imide positions. Indeed, following this approach, many water-soluble perylenediimide derivatives have been prepared, and some of them have photosensitized the formation of singlet oxygen and phototoxicity against cancer cells.[23,24,25] In the case of the complex reported here, solubility in organic solvents and in water is assigned to the $\{Ru(phen)_3\}^{2+}$ moiety,[21] whereas self-aggregation together with the potential of the complex to PDT is the subject of this work.

To explore the intermolecular interactions of $[Ru(phen)_2(pPDIp)]^{2+}$, we considered the UV-vis and emissive spectroscopic behavior of complex in buffer solution (pH 7.4), in cell culture medium (RPMI) and immobilized in starch films in the dark. We also evaluated the extent and implications of aggregation on the photochemical and photophysical properties of the complex in these media. For comparison, the studies were also performed in dimethylsulfoxide (DMSO) solution.

Our results indicate that the solvent influences the aggregation process that markedly affects the photochemical and photophysical processes. A direct consequence of this effect is that we can use solvent and irradiation wavelength to tune the excited state energy and, consequently, select the desired product. For example, in DMSO, the $pPDIp^{\bullet-}$ radical anion forms of the pPDIp moiety are obtained regardless of irradiation wavelength within the absorption envelope, whereas formation of $pPDIp^{\bullet-}$ at 518 nm irradiation and both $pPDIp^{\bullet-}$ and $pPDIp^{2-}$ at 420 nm irradiation is reached in RPMI solution. In contrast, in buffer solution (pH 7.4) and starch films, the aggregation process increases significantly in such way that it prevents the photochemical process, but leads to population of the ^{3*}pPDIp. In all solvents investigated the solution returns to its original spectrum when the light is turned off.

The results also indicated an interesting profile of biological activity with singlet oxygen activation in buffer solution, with strong photocytotoxicity in vitro cell proliferation inhibition of B16F10-Nex2 cells under green LED (518 nm, 0.41 J/cm^2) displaying IC_{50} values of 1.2 ± 0.1 μmol L^{-1}. No significant effects on cell viability were found in the dark at 0.1 to 10 μmol L^{-1} of complex with incubation period of 24 h.

2. Results and Discussion

2.1. Influence of the Medium on Optical Properties

2.1.1. DMSO Solution

Absorption and emission spectra of $[Ru(phen)_2(pPDIp)]^{2+}$, $[Ru(phen)_3]^{2+}$ complexes and pPDIp free ligand are shown in Figure S1 in the Supporting Information. The absorption spectrum in the visible region of the $[Ru(phen)_2(pPDIp)]^{2+}$ complex consists of contributions of both chromophores the pPDIp and the parent complex $[Ru(phen)_3]^{2+}$, indicative of overlapping transitions to π–π* and MLCT states. Apart from these bands, a new weak and broad absorption that resembles the perylenediimide in the radical anion forms ($PDI^{\bullet-}$) appears around 700 nm.[26,27] In agreement, the EPR spectrum of $[Ru(phen)_2(pPDIp)]^{2+}$ complex and free pPDIp ligand displays an EPR signal centered at $g = 2.0035$, attributed in the literature[26,27] to the chemically produced $PDI^{\bullet-}$ (Figure S2). The radical anion concentration in the free pPDIp ligand was determined through integration of the EPR signals to produce 30%. The amount of radical anion is drastically decreased in the complex to produce approximately 2% of the total amount.

By excitation at 450 nm or 500 nm, the emission spectrum of complex also consists of contributions of both chromophores the ^{3*}MLCT phosphorescence corresponding to the $\{Ru(phen)_3\}^{2+}$core and the fluorescence of the pPDIp core (Figure S1). The emission lifetime of complex was investigated using a time-resolved single photon counting equipment, with $\lambda_{exc} = 448$ nm. The emission decay profiles required a tri-exponential fit, suggesting the presence of three emitting processes, 0.99 ns (12.3% of total emission), 4.5 ns(12.6%), and 392.7 ns (75.1%), $\chi^2 = 1.1$ (Figure S3) with the ^{3*}MLCT of $\{Ru(phen)_3\}^{2+}$ moiety dominating the emission decays.

The complex is photoreactive and the changes in the absorption spectrum are consistent with generation of the

pPDIp$^{\bullet-}$ radical anion (Figure 2). Exhaustive photolysis produced a final stable spectrum of radical anion. Back-reaction is observed when the light is turned off. Similar results are obtained when photolysis is performed using an open cuvette (without lid), although formation of radical anion is less efficient (Figure S4).

Photolysis monitored by EPR also shows a growth of the radical anion species. After 50 min irradiation with a 420 nm light, the percentage of radical anion was 33% of the total amount of complex (25 μmol L^{-1}). At the end of photolysis, a well-resolved multiline EPR spectrum with g = 2.0031 was obtained, attributed to pPDIp$^{\bullet-}$, as shown in Figure 2B (inset). The EPR simulated spectrum calculated by adjusting the parameters with eight hydrogen nuclei and two nitrogen nuclei confirmed the delocalization of the unpaired electron in the aromatic rings of the pPDIp component. The simulation was obtained using a Gaussian line shape with linewidth of 0.37 G and hyperfine parameters 1.78 G and 1.81 G for the two nitrogen nuclei and 0.700 G, 0.688 G, 0.652 G, 0.594 G, 0.581 G, 0.571 G, 0.568 G, 0.421 G, for the eight hydrogen nuclei. The Gaussian line shape and the well-resolved hyperfine splitting indicates that no aggregation of pPDIp$^{\bullet-}$ occurs during photolysis.

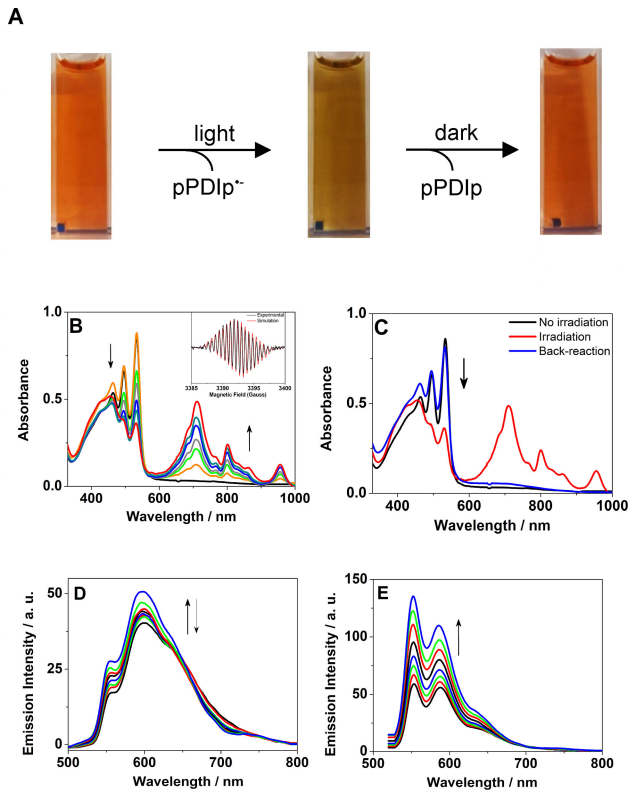

Figure 2. Photolysis of complex (25 μmol L^{-1}) with 420 nm light in deaerated DMSO solution, total irradiation time = 180 min. A) Photos of solution before and after photolysis and after the back reaction. B)Visible spectral changes during photolysis as monitored by UV/Vis absorption spectroscopy; Inset: Experimental (black) and simulated (red) EPR spectra after 50 min of photolysis. C) Visible spectral changes during the back reaction. D)Emission spectral changes monitored by excitation at 450 nm and E) 500 nm.

Photolysis with 420 nm light accompanied by the emission spectrum at 500 nm excitation shows an increase in the intensity of the 0–0 emission peak relative to 0–1, whereas the MLCT emission monitored at 450 nm decreases (Figure 2). Continuous photolysis experiments carried out with 518 nm light irradiation led to similar spectroscopic results (Figure S5).

2.1.2. RPMI Solution

The spectroscopic, photophysical and photochemical properties of the [Ru(phen)$_2$(pPDIp)]$^{2+}$ complex changed when DMSO was replaced by RPMI solution (Figure S6). A short red shift and an inversion on the intensity of the 0–0 peak relative to 0–1 in the absorption spectrum of complex are observed. Compared with the DMSO, these changes are indicative of a weakly coupled H-type aggregation, as found in PDI derivatives.[28]

Aggregation is also reflected in the emission spectrum of [Ru(phen)$_2$(pPDIp)]$^{2+}$. The MLCT (Ru→phen) emission is well preserved and dominated the entire spectrum, i.e., it is independent of excitation wavelength, whereas the pPDIp core fluorescence is almost completely suppressed (Figure S6). The emission kinetic decays could be fit to a tri-exponential curve similar to that of the DMSO solution, whereas an increase in both lifetime and emission contribution in the ^{3*}MLCT of {Ru(phen)$_3$}$^{2+}$ were observed: τ = 0.46 ns (0.2%); 4.14 ns (11.3%); 622.6 ns (88.5%); χ^2 = 1.1 (Figure S3).

When deaerated solutions of the [Ru(phen)$_2$(pPDIp)]$^{2+}$ complex were subject to continuous photolysis at 518 nm light, the resulting optical spectral changes were consistent with formation of the pPDIp$^{-\bullet}$ radical anion, whereas irradiation at 420 nm originated a final spectrum consistent with formation of the pPDIp$^{-\bullet}$ and the pPDIp^{2-} dianion[29] (exhibiting an broad absorption at 650 nm; Figure 3). Interestingly, in the course of photolysis at 420 nm, the emission spectrum (MLCT band) decreases in intensity; however, an unstable decrease and increase in the MLCT emission spectrum was detected with light irradiation at 518 nm (Figure 3).

To probe these events in more detail, photolysis was performed with 518 nm to generate the pPDIp$^{\bullet-}$, then irradiation was stopped and the light irradiation was changed to 420 nm. The UV/Vis absorption spectral changes exhibited the pPDIp^{2-} dianion absorption (Figure S7). As previously observed, back-reaction occurs when the light is turned off either at 420 or 518 nm light irradiation.

The amount of radical anion formed was determined after exhaustive photolysis by EPR spectroscopy to produce 5% of the total amount of complex irradiated at 420 nm and 2% at 518 nm. This value is comparable to those found before photolysis. In agreement, no hyperfine splitting was detected during photolysis monitored by EPR (Figure 3). This absence of well-resolved hyperfine splitting for the pPDIp radical anions in RPMI indicates that the distribution of the unpaired electron is spread over a larger π-surface in comparison with that in DMSO. Electron sharing over multiple PDI subunits within nanowire DNA hairpins and a molecular triangle result in a similar loss of spectroscopic hyperfine structure.[30,31] Photolysis

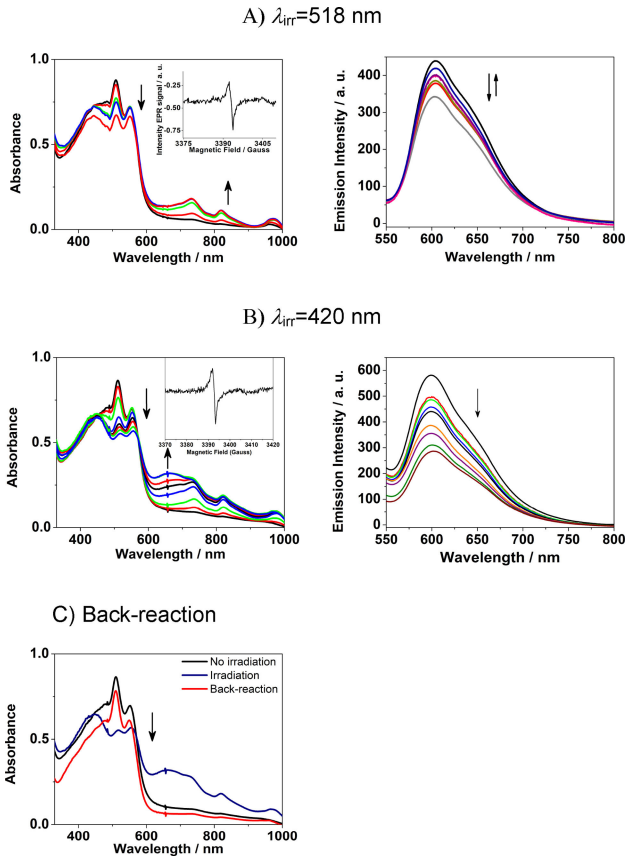

Figure 3. Photolysis of $[Ru(phen)_2(pPDIp)]^{2+}$ complex (50 μmol L^{-1}) in deaerated RPMI solution, total irradiation time = 180 min, irradiating at 518 nm (A) and 420 nm (B). Change in the UV/Vis absorption spectra (left; Inset in (A, left) and (B, left): Experimental EPR spectrum after 50 min of photolysis) and emission spectra (right) monitored at 450 nm. C) UV/Vis absorption spectra showing the back-reaction product.

of the complex is completely suppressed when performed using an open cuvette (without lid; Figure S8).

2.1.3. Buffer pH 7.4 Solution and Starch Film

The UV/Vis absorption and emission spectra of the $[Ru(phen)_2(pPDIp)]^{2+}$ complex in buffer solution pH 7.4 are similar to those found in RPMI (Figure S6). Fluorescence of the pPDIp core is suppressed, whereas phosphorescent emission of the $\{Ru(phen)_3\}^{2+}$ core is preserved. As observed in RPMI, the emission decay profile in buffer solution pH 7.4 required a tri-exponential fit (Figure S3). The population of ^{3*}MLCT (504 ns, 99%) is higher compared with that of the RPMI while the ^{1*}LLCT (5.0 ns, 0.25%) of pPDIp core is similar. A short emission lifetime of 37 ns (0.26%) indicates formation of an excimer, as observed in similar systems.[32]

It is worth noting that formation of the radical anion moiety was not detected by UV/Vis absorption spectroscopy during photolysis (Figure S9), demonstrating that the solvent influences the aggregation process that affects the photochemical process directly.

When the complex was immobilized in starch film, the absorption spectrum corresponding to the pPDIp moiety became more unstructured, the fluorescence was completely suppressed while the emission of $\{Ru(phen)_3\}^{2+}$ moiety was red shifted by 50 nm, indicating strong intermolecular interactions (Figure 4). The fit of the emission decay profiles to a tri-

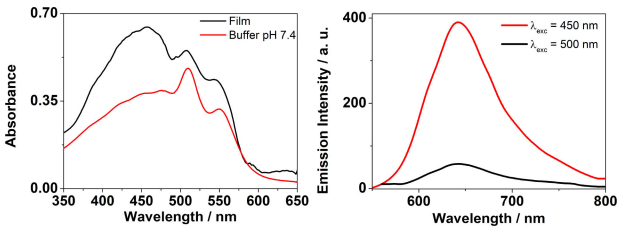

Figure 4. Absorption and emission spectra of the $[Ru(phen)_2(pPDIp)]^{2+}$ complex in starch film and buffer solution in the dark.

exponential curve resulted in reduced-χ^2 values equal to 1.0 and random distribution of residuals (Figure S3). The decays were described by very long lifetime, 1.66 μs, that accounts for 96.03% of the total emission, 351 ns (3.95%), and a short lifetime component, 1.85 ns (0.02%). The long lifetime is in excellent agreement with previous values reported for acetonitrile solution.[21] In this previous work, the long lifetime was attributed to the long-lived triplet ^{3*}pPDIp (1.8 μs) produced by charge recombination of the intermediate excited species $\{(phen)_2Ru(III)(pPDIp^{\bullet-})\}$. In acetonitrile solution, the ^{3*}pPDIp sensitized the formation of the singlet molecular oxygen, with quantum yield values of 0.57.[21] As it will be shown in the biologic stuies section, $^1O_2$ was also detected and quantified in buffer solution and starch films.

The solvent intermediates the π–π self-assembly in DMSO, RPMI, buffer pH 7.4, and starch film through different intermolecular interactions, with an impact on the observed photophysical and photochemical properties displayed by the assemblies.

The photochemical generation of the $pPDIp^{\bullet-}$ radical anion of the pPDIp moiety observed without addition of a reducing agent demonstrates the strong π-acceptor ability of the pPDIp ligand, which can be attributed to the functionalization of the axial positions of perylenediimide with two phenanthrolines. They provide delocalization of electron density into the PDI unity and limit the electron mobility to the aromatic ring of the PDI, which acts as an "electron sink". In donor solvents such as DMSO, the photochemical reduction of pPDIp is probably facilitated by the interactions of bulk solvent with the hydrogen of the aromatic pPDIp ring. Similar behavior has been recently observed for PDI and NDI modified derivatives.[33,34]

RPMI induces a π–π interaction in the ground state. Consequently, excimer formation is highly facilitated. Moreover, in RPMI, the photolysis is wavelength dependent, suggesting that the lowest MLCT and ILCT states are reasonably close in energy. These results support the population of a specific excited state at the chosen irradiation wavelength. In addition, it is also expected that the solvent have a large impact on the

rates of nonradiative deactivation. Unambiguously, the large intermolecular interactions observed when the complex was immobilized in starch films led to the population of the triplet pPDIp excited state, presenting longer fluorescence.

2.2. Direct Detection and Quantification of Singlet Oxygen by Light Irradiation of $[Ru(phen)_2(pPDIp)]^{2+}$

Whereas ^{3*}pPDIp is implied by spectroscopic experiments, detection and quantification of singlet oxygen and/or its reactive species is needed to indicate the potential of complex in PDT in physiologic medium. The photo-activation of $^1O_2$ was investigated using the EPR technique employing spin trapping 2,2,6,6-tetramethyl-4-piperidinol (TMP-OH). In the presence of $^1O_2$, TMP-OH is oxidized to 4-hydroxy-2,2,6,6-tetramethylpiperidine-N-oxyl (TEMPOL).[35,36]

The experiments were conducted in buffer solution (pH 7.4) in a flat cell without oxygen bubbling. In the dark, the EPR spectrum of TMP-OH in the presence of complex shows a signal at 3393 G that corresponds to 0.33% of complex concentration. This amount is negligible compared with the total amount of the complex. Indeed, the intensity of this signal was not affected by irradiation; it remained constant during photolysis.

The EPR spectra measured during photolysis of the $[Ru(phen)_2(pPDIp)]^{2+}$ complex displayed three lines with the same intensity, which match the simulated spectra of the nitroxide radical. This result is consistent with formation of the TEMPOL radical (Figure 5).

The EPR spectral changes during photolysis show that the intensity of the TEMPOL signal increases with the concentration of complex, and it is also dependent on the wavelength and time of light irradiation. To establish the concentration of the $^1O_2$ generated with the time of irradiation, a calibration curve was built with TEMPO as a standard (Figure S10). Figure 5 and Table S1 show that the concentration of $^1O_2$ increased in the course of photolysis of complex.

Analogous experiments were performed using DMPO to trap possible reactive oxygen species: superoxide radical and/or hydroxyl.[37] There was no observable DMPO/$^{\bullet}$OOH adduct signal under the conditions used in the experiments discussed here. The most probable candidate would be the $\{Ru(phen)_2(pPDIp)^{3*}\}$.

The 420 nm light irradiation of a thin starch film of $[Ru(phen)_2(pPDIp)]^{2+}$ (100 μmol L^{-1}) in contact with D_2O solution containing TMP-OH also yields the signals attributed to TEMPOL. For comparison, photolysis of the starch film of $[Ru(phen)_2(pPDIp)]^{2+}$ (100 μmol L^{-1}) was performed under the same experimental conditions, with 518 nm LED illumination and sunlight in buffer solution (pH 7.4). Efficiency of the $[Ru(phen)_2(pPDIp)]^{2+}$ complex under these different conditions is demonstrated in Figure 6. It can be seen that $^1O_2$ is generated in all conditions tested. However, at a distance of 0.5 cm between the film and the surface of the TMP-OH, $^1O_2$ formation was impaired, which means that direct contact between solution and the $[Ru(phen)_2(pPDIp)]^{2+}$ film is necessary.

These results demonstrated that $^1O_2$ is formed under visible light irradiation either dissolved in aqueous solution or immobilized in starch films. This opens an opportunity for the potential application of this complex in several areas of science.

We explored the potential applications of the $[Ru(phen)_2(pPDIp)]^{2+}$ complex in PDT in vitro experiments using the B16F10-Nex2 murine melanoma cells.

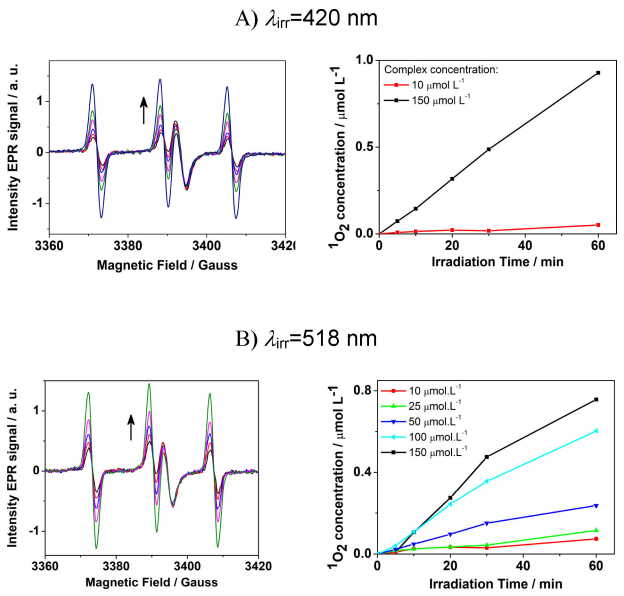

Figure 5. Comparative production of $^1O_2$ using light sources of different wavelengths during irradiation of the $[Ru(phen)_2pPDIp]^{2+}$ complex in buffer solution (pH 7.4). $^1O_2$was indirectly detected by EPR spectroscopy (left spectra) using the spin trap TMP-OH, which forms TEMPOL as a final species.

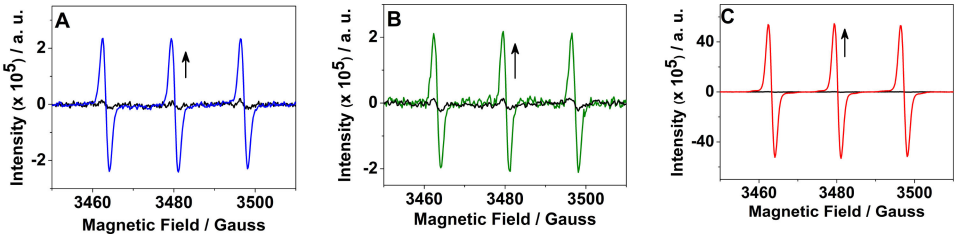

Figure 6. Comparative production of TEMPOL generated from irradiation of a starch film loaded with the $[Ru(phen)_2(pPDIp)]^{2+}$ complex (100 μmol L^{-1}) in contact with a D_2O solution containing TMP-OH: A) 420 nm, B) 518 nm, and C) sunlight. $^1O_2$was indirectly detected by EPR spectroscopy using the spin trap TMP-OH, which forms TEMPOL as a final species.

2.3. Dark- and Photocytotoxicity of $[Ru(phen)_2(pPDIp)]^{2+}$ towards B16F10-Nex2 Cells

The viability of B16F10-Nex2 murine melanoma cell line in the dark and under light irradiation were evaluated using the MTT assay.

2.3.1. Dark Cytotoxicity of $[Ru(phen)_2(pPDIp)]^{2+}$

The dark cytotoxicity of $[Ru(phen)_2(pPDIp)]^{2+}$ incubated with B16F10-Nex2 cells for 24 h was investigated over a range of concentrations between 0.1 and 100 μmol L^{-1}. Cells without the complex were maintained as controls. The percentages of cell survival were calculated relative to the control cells and the results are presented in Figure 7. These data indicated that

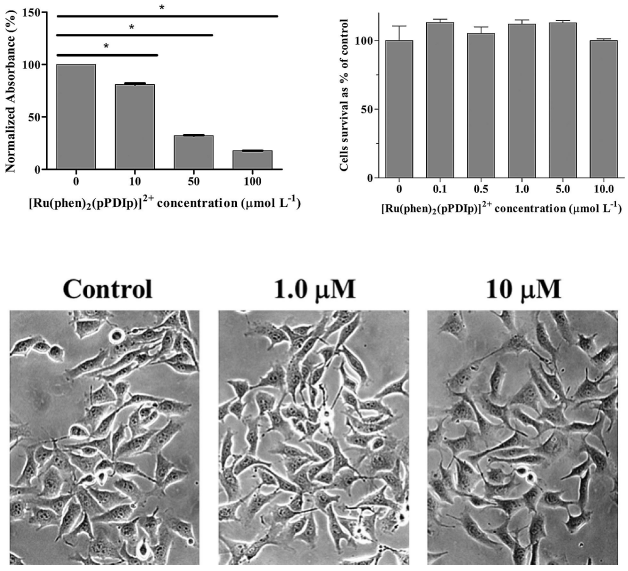

Figure 7. Dark cytotoxicity of the $[Ru(phen)_2(pPDIp)]^{2+}$ complex towards B16F10-Nex2 cells incubated for 24 h without irradiation (top). Morphological changes in cells after 24 h incubation with the complex in the dark (bottom).

$[Ru(phen)_2(pPDIp)]^{2+}$ showed an IC_{50} value of 28 μmol L^{-1} under no light irradiation. No significant dark cytotoxicity at concentrations $\leq$10 μmol L^{-1}, with no apparent changes in the morphology of cells incubated with complex were visualized under these conditions (Figure 7).

2.3.2. Photocytotoxicity of 420 nm Light

The photocytotoxic effect of 420 nm light on superficial tumor including B16F10 melanoma cell line is well reported.[38,39] For this reason, we initially conducted experiments to evaluate the effect of irradiation using our photochemical system (blue light, 420 nm, 1.96 mW/cm^2) on the B16F10-Nex2 cell viability.

An immediate photocytotoxic effect was obtained after30 min irradiation (light dose of 3.52 J/cm^2) to produce74.85% (± 0.02) cell viability. In contrast, no significant photocytotoxic effect was noted with 5 min light irradiation (light dose of 0.5 J/cm^2; Figure S11).

2.3.3. Photocytotoxicity of $[Ru(phen)_2(pPDIp)]^{2+}$ with 420 nm Light

The effect of complex on cell viability was assessed immediately after 30 min irradiation (3.52 J/cm^2). Figure S12 shows that a concentration of $[Ru(phen)_2(pPDIp)]^{2+}$as little as 0.1 μmol L^{-1} caused near 100% inhibition of cell viability. Shorter periods of irradiation also caused photocytotoxic effect on cell viability. For example, the IC_{50} value measured after 24 h of treatment with 5 min irradiation (0.58 J/cm^2) was 0.5 ± 0.16 μmol L^{-1}. Figure S13 shows the changes in cell morphology, which are mostly associated to apoptosis.[40] The cells became rounded, shrank, and exhibited expressive loss of volume that increased with increasing the concentration of complex.

2.3.4. Photocytotoxicity of Green LED (518 nm, 0.23 mW/cm^2)

No effects on B16F10-Nex2cell viability was observed 24 h after treatment with green LED using light doses of 0.069, 0.207, and 0.414 J/cm^2, respectively (Figure S14).

2.3.5. Photocytotoxicity of $[Ru(phen)_2(pPDIp)]^{2+}$ with a Green LED

Upon light irradiation, the cells incubated with complex underwent expressive loss of viability, which was dependent on light dose and complex concentration. For example, at 30 min irradiation (light dose of 0.41 J/cm^2) the IC_{50} value reached was 1.2 μmol L^{-1} (Figure 8).

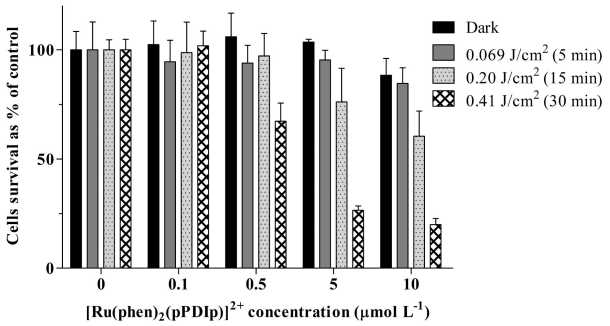

Figure 8. Influence of the light dose and $[Ru(phen)_2(pPDIp)]^{2+}$ concentration on the photocytotoxicity towards B16F10-Nex2 melanoma cells. The $[Ru(phen)_2(pPDIp)]^{2+}$ complex was primarily incubated with the cells for a period of 4 h, followed by irradiation by a green LED light (518 nm) in different doses. The cell viability was evaluated after 24 h of irradiation treatment.

3. Conclusions

The present study demonstrates that the $[Ru(phen)_2(pPDIp)]^{2+}$ complex meets several key goals for the design of a photosensitizer for melanoma cancer treatment. This complex is stable and retains its phosphorescence in buffer solution and on starch film, yet it displays high photoactivation of singlet oxygen. Furthermore, the complex presents no cytotoxicity up to 10 $\mu mol\,L^{-1}$ and high photocytotoxicity towards B16F10-Nex2 murine melanoma cells under a low dose of green LED, 518 nm. Therefore, the $[Ru(phen)_2(pPDIp)]^{2+}$ complex is a promising candidate for singlet oxygen photoactivation in topical applications with LED excitation source.

Experimental Section

Materials

Solvents used for spectroscopic measurements were spectrophotometric grade. The reagents were purchased from Sigma-Aldrich. Cassava starch was kindly supplied by Cargill (São Paulo, Brazil), containing 19.7% of amylose.

Instrumentation

Absorption spectra were recorded on an Agilent 8453 UV-vis spectrophotometer. Emission spectra were recorded in a Shimadzu RF-5301PC fluorescence spectrophotometer. Fluorescence intensity decay was obtained using the time-correlated single photon counting (TCSPC) technique. The excitation source was a titanium–sapphire laser (Tsunami 3950, Spectra Physics) pumped by the solid-state laser Millenia Xs (Spectra Physics). The pulse repetition rate was adjusted by a Pulse Picker 3986 (Spectra Physics). The excitation wavelength was chosen with the aid of harmonic generators with the Flexible Harmonic Generator (Spectra Physics), which was directed to an Edinburgh FL900 spectrometer. A refrigerated Hamamatsu C4878 micro-channel plate photomultiplier detected the emitted photons, and software provided by Edinburgh Instruments was used to analyze the decays by fitting to multi-exponential curves. All spectroscopic measurements were conducted in 1cm quartz cuvettes (Hellma, Germany) at room temperature and the solutions were deaerated through bubbling with high-purity nitrogen for at least 30 min.

Light Sources

The following light systems were used in this study: a homemade mobile photochemical reactor with Rayonet lamps (model RMR-4200Å) using a 1.96 mW/cm^2 fluence rate and a green LED array composed of 18 LEDs connected in series (model SMD 5050, $\lambda =$ 518 nm) using a 0.23 mW/cm^2 fluence rate. Spectral emission for the light system were recorded using a spectrometer (USB2000+, Ocean Optics Inc.).

Synthesis of the $[Ru(phen)_2(pPDIp)]^{2+}$ Complex

This complex was prepared according to procedure described in the literature.[21]

Preparation of Starch Films

The films were prepared following previously published procedures.[41] Cassava starch (470 mg) with 75 mg of glycerol was dissolved in 7.0 mL deionized water and heated up to 75 °C under stirring for gelatinization. After that, the solution of the $[Ru(phen)_2(pPDIp)]^{2+}$ complex in ethanol/water (30% of ethanol) (100 $\mu mol\,L^{-1}$) was mixed with the gelatinized starch suspension and, after homogenization, the solution was poured onto cylindrical plates. Then the films were dried in oven at 40 °C for approximately 24 h. Films were stored at controlled relative humidity of 75% at ambient temperature (23 ± 2 °C). The immobilization of $[Ru(phen)_2(pPDIp)]^{2+}$ into the film was verified by UV-vis and emission spectroscopy.

Photolysis

Solutions of complex the $[Ru(phen)_2(pPDIp)]^{2+}$ complex (25–50 $\mu mol\,L^{-1}$) (3 mL) were rigorously deoxygenated using high-purity nitrogen atmosphere and then irradiated with 420 nm or 518 nm light using a 1 cm path length, four clear-sided quartz cell. Photolysis progress was monitored by UV-vis, emission and EPR spectroscopy. During photolysis, the solution in the cell was irradiated for defined time periods. The samples were rapidly stirred to ensure uniform absorption throughout the cell.

Electron Paramagnetic Resonance (EPR) Spectroscopy

EPR measurements were performed in a Varian E109 series X band spectrometer operating at 9.5 GHz. The concentrations of the radical species and the g value of the free ligand and the $[Ru(phen)_2(pPDIp)]^{2+}$ complex solutions in the dark and after photolysis were determined using MgO standard doped with Cr(III). Deaerated solutions in DMSO and RPMI media at 150–50 $\mu mol\,L^{-1}$ were transferred to a flat quartz cell containing the Cr(III) standard, fixed outside, during all measurements. Each solution was irradiated with 420 nm or 518 nm light for certain time intervals. The relation between the sample areas of the spectra and the area of the signal of the standard was used to calculate the number of spins and, consequently, the number of molecules with unpaired electrons. EPR conditions are as follows: microwave power, 20mW; modulation amplitude, 0.25 G; time constant, 0.0165 s; 1 scan.

Singlet Oxygen Measurements

EPR spin-trapping spectroscopy was used to measure $^1O_2$ production. Experimental solutions were prepared by mixing the $[Ru(phen)_2(pPDIp)]^{2+}$ complex (10–150 $\mu mol\,L^{-1}$) with2,2,6,6-tetramethyl-4-piperidinol (TMP-OH) (48 $mmol\,L^{-1}$) in potassium phosphate buffer (pH 7.4) in a total volume of 200 µL. The solutions were irradiated in the flat quartz cell in the EPR cavity with 420 nm or 518 nm light for defined time periods at room temperature. EPR conditions are as follows: microwave power, 20 mW; modulation amplitude, 0.25 G; time constant, 0.128 s; 16 scans. The EPR experimental spectra were simulated and the intensity of signal by measuring the relative area of the EPR absorption simulated spectrum. The concentration of $^1O_2$ was established from calibration curve using the 4-Hydroxy-TEMPO (TEMPO) in aqueous buffer phosphate solution (pH 7.4) (10–0.1 $\mu mol\,L^{-1}$) as a standard and analyzed under similar experimental conditions.

Cell Culture

The B16F10-Nex2 melanoma murine cell line was cultured in RPMI 1640 medium (Gibco) supplemented with 10 $mmol\,L^{-1}$ HEPES(4-(2-

hydroxyethyl)-1-piperazineethanesulfonic acid) (Sigma-Aldrich), 24 mmol L^{-1} sodium bicarbonate (Sigma-Aldrich), 40 mg/mL gentamicin (Hipolabor), and 10% (v/v) fetal bovine serum (FBS, Life Technologies) under humidified atmosphere at 37 °C and 5% CO_2.

Dark- and Photoinduced Cytotoxicity

The cells were seeded into a 96-well plate at a density of $\sim 2 \times 10^3$ per well. After overnight incubation, the cells were washed with PBS and 200 μL RPMI medium containing the $[Ru(phen)_2(pPDIp)]^{2+}$ complex at varying concentrations (between 0.1–100 μmol L^{-1}) was added for set incubation periods. For determination of dark cytotoxicity the cells were incubated with the $[Ru(phen)_2(pPDIp)]^{2+}$ complex for 24 h in the dark, whereas for light-dependent cytotoxicity, the cells were incubated for 4 h before the light stimulus. The plates were irradiated using 420 nm or 518 nm light with different light dosages. Cell cytotoxicity levels immediately after irradiation and 24 h after treatment were determined using the 3-(4,5-dimethylthiazol-2-yl)-2,5-diphenyltetrazolium bromide (MTT) assay: cells were incubated with medium containing MTT (0.5 mg/mL) for 4 h. The formazan derivative insoluble product was dissolved with 100 μL of 10% SDS solution with 0.01 mol L^{-1} HCl. After incubation for 16 h, absorbance was quantified at 570 nm with reference filter of 650 nm, using a 96-well plate reader Spectramax M2e device (Molecular Devices). All measured data were processed and analyzed using GraphPad Prism software (GraphPad Software, Inc., California, USA). Data were presented as means ± standard deviation (SD) of four independent absorbance measurements, normalized to 100% viability of the untreated control.

Acknowledgements

The authors are grateful to FAPESP (Proc. no. 2017/00839-1, 2016/09633-4) and CNPq (Proc. no. 305668/2014-5) for the financial support. We would also like to thank Professor Luciano Bachmann for the spectral emission measurements for the light systems investigated (IF-FFCLRP-USP) and the inorganic chemistry group of Instituto de Química de São Carlos (USP) for the initial EPR experiments.

Conflict of Interest

The authors declare no conflict of interest.

Keywords: perylene diimide · photosensitizer · ruthenium · singlet oxygen · solvent effects

[1] E. Christensen, C. Mørk, E. Skogvoll, *Br. J. Dermatol.* **2012**, *166*, 1342–1348.
[2] R. R. Allison, C. H. Sibata, *Photodiagn. Photodyn. Ther.* **2010**, *7*, 61–75.
[3] L. R. Braathen, R. M. Szeimies, N. Basset-Seguin, R. Bissonnette, P. Foley, D. Pariser, R. Roelandts, A. M. Wennberg, C. A. Morton, *J. Am. Acad. Dermatol.* **2007**, *56*, 125–143.
[4] A. H. Arits, K. Mosterd, B. A. Essers, E. Spoorenberg, A. Sommer, M. J. De Rooij, H. P. van Pelt, P. J. Quaedvlieg, G. A. Krekels, P. A. van Neer, J. J. Rijzewijk, A. J. van Geest, P. M. Steijlen, P. J. Nelemans, N. W. Kelleners-Smeets, *Lancet Oncol.* **2013**, *14*, 647–654.
[5] P. Savoia, T. Deboli, A. Previgliano, P. Broganelli, *Int. J. Mol. Sci.* **2015**, *16*, 23300–23317.
[6] M. T. Wan, J. Y. Lin, *Clin. Cosmet. Investig. Dermatol.* **2014**, *7*, 145–163.
[7] N. Shishkova, O. Kuznetsova, T. Berezov, *Cancer Biol Med.* **2012**, *9*, 9–17.
[8] N. Yavari, S. Andersson-Engels, U. Segersten, P. U. Malmstrom, *Can. J. Urol.* **2011**, *18*, 5778–5786.
[9] R. Cosgarea, M. Susan, M. Crisan, S. Senila, *J. Eur. Acad. Dermatol. Venereol.* **2013**, *27*, 980–984.
[10] R. Saini, N. V. Lee, K. Y. P. Liu, C. F. Poh, *Cancers.* **2016**, *8*, 83.
[11] M. Machacek, A. Cidlina, V. Novakova, J. Svec, E. Rudolf, M. Miletin, R. Kucera, T. Simunek, P. Zimcik, *J. Med. Chem.* **2015**, *58*, 1736–1749.
[12] X.-M. Shen, B.-Y. Zheng, X.-R. Huang, L. Wang, J.-D. Huang, *Dalton Trans.* **2013**, *42*, 10398–10403.
[13] X. Q. Zhou, L. B. Meng, Q. Huang, J. Li, K. Zheng, F. L. Zhang, J. Y. Liu, J. P. Xue, *ChemMedChem.* **2015**, *10*, 304–301.
[14] K. Mitra, S. Gautam, P. Kondaiah, A. R. Chakravarty, *ChemMedChem.* **2016**, *11*, 1956–1967.
[15] C. Mari, V. Pierroz, S. Ferrari, G. Gasser, *Chem. Sci.* **2015**, *6*, 2660–2686.
[16] C. R. Cardoso, M. V. S. Lima, J. Cheleski, E. J. Peterson, T. Venâncio, N. P. Farrell, R. M. Carlos, *J. Med. Chem.* **2014**, *57*, 4906–4915.
[17] E. S. Antonarakis, A. Emadi, *Cancer Chemother. Pharmacol.* **2010**, *66*, 1–9.
[18] F. Schmitt, P. Govindaswamy, G. Süss-Fink, W. H. Ang, P. J. Dyson, J. Juillerat-Jeanneret, B. Therrien, *J. Med. Chem.* **2008**, *51*, 1811–1816.
[19] J.-X. Zhang, J.-W. Zhou, C.-F. Chan, T. C.-K. Lau, D. W. J. Kwong, H.-L. Tam, N.-K. Mak, K.-L. Wong, W.-K. Wong, *Bioconjugate Chem.* **2012**, *23*, 1623–1638.
[20] U. Schatzschneider, *Eur. J. Inorg. Chem.* **2010**, *2010*, 1451–1467.
[21] E. R. Santos, J. Pina, T. Venâncio, C. Serpa, J. M. G. Martinho, R. M. Carlos, *J. Phys. Chem. C.* **2016**, *120*, 22831–22843.
[22] W. Sun, L. M. Schuchter, *Curr. Treat Options Oncol.* **2001**, *2*, 193–202.
[23] R. Bonnet, G. Martinez, *Tetrahedron.* **2001**, *57*, 9513–9547.
[24] S. K. Yang, X. Shi, S. Park, S. Doganay, T. Ha, S. C. Zimmerman, *J. Am. Chem. Soc.* **2011**, *133*, 9964–9967.
[25] A. Margineanu, J. Hofkens, M. Cotlet, S. Habuchi, A. Stefan, J. Qu, C. Kohl, K. Müllen, J. Vercammen, Y. Engelborghs, T. Gensch, F. C. De Schryver, *J. Phys. Chem. B.* **2004**, *108*, 12242–12251.
[26] Y. Jiao, K. Liu, G. Wang, Y. Wang, X. Zhang, *Chem. Sci.* **2015**, *6*, 3975–3980.
[27] D. Schmidt, D. Bialas, F. Würthner, *Angew. Chem. Int. Ed.* **2015**, *54*, 3611–3614; *Angew. Chem.* **2015**, *127*, 3682–3685.
[28] F. C. Spano, *Acc. Chem. Res.* **2010**, *43*, 429–439.
[29] D. Gosztola, M. P. Niemczyk, W. Svec, A. S. Lukas, M. R. Wasielewski, *J. Phys. Chem. A.* **2000**, *104*, 6545–6551.
[30] T. M. Wilson, T. A. Zeidan, M. Hariharan, F. D. Lewis, M. R. Wasielewski, *Angew. Chem. Int. Ed.* **2010**,*49*, 2385–2388; *Angew. Chem.* **2010**, *122*, 2435–2438.
[31] N. J. Schuster, D. W. Paley, S. Jockusch, F. Ng, M. L. Steigerwald, C. Nuckolls, *Angew. Chem. Int. Ed. Engl.* **2016**, *55*, 13519–13523.
[32] P. E. Hartnett, S. M. Dyar, E. A. Margulies, L. E. Shoer, A. W. Cook, S. W. Eaton, T. J. Marks, M. R. Wasielewski, *Chem. Sci.* **2015**, *6*, 402–411.
[33] R. Kang, R. Miao, Y. Qi, X. Chang, C. Shang, L. Wang, Y. Fang, *Chem. Commun.* **2017**, *53*, 10018–10021.
[34] Q. Song, F. Li, Z. Wang, X. Zhang, *Chem. Sci.* **2015**, *6*, 3342–3346.
[35] H. Huang, P. Zhang, B. Yu, C. Jin, L. Ji, H. Chao, *Dalton Trans.* **2015**, *44*, 17335–17345.
[36] A. Prasad, U. Ferretti, M. Sedlářová, P. Pospíšil, *Sci. Rep.* **2016**, *6*, 20094.
[37] A. Sparsa, K. Faucher, V. Sol, H. Durox, S. Boulinguez, V. Doffoel-Hantz, C. A. Calliste, J. Cook-Moreau, P. Krausz, F. G. Sturtz, C. Bedane, M. O. Jauberteau-Marchan, M. H. Ratinaud, J. M. Bonnetblanc, *Anticancer Res.* **2010**,*30*, 143–147.
[38] S. Vandersee, M. Beyer, J. Lademann, M. E. Darvin, *Oxid. Med. Cell Longev.* **2015**, *2015*, 579675.
[39] C. D. Bortner, J. A. Cidlowski, *Cell Death Differ.* **2002**, *9*, 1307–1310.
[40] J. J. Bright, A. Khar, *Biosci. Rep.* **1994**, *14*, 67–68.
[41] H. F. Aguiar, A. C. Roveda, R. J. Piva, K. A. Onoda, A. A. Miyakawa, J. E. Krieger, D. W. Franco, C. C. Tadini, *J. Appl. Polym. Sci.* **2015**, *132*, 41382.

Manuscript received: February 1, 2018
Accepted Article published: April 18, 2018
Version of record online: May 18, 2018